Determination of spin relaxation times in heavy metals via second-harmonic spin injection magnetoresistance

C. Fang, C. H. Wan, B. S. Yang, J. Y. Qin, B. S. Tao, H. Wu, X. Zhang, X. F. Han, A. Hoffmann, X. M. Liu, and Z. M. Jin

Determination of spin relaxation times in heavy metals via 2nd harmonic spin injection magnetoresistance

C. Fang, C. H. Wan,* B. S. Yang, J. Y. Qin, B. S. Tao, H. Wu, X. Zhang, and X. F. Han†

Institute of Physics, Chinese Academy of Sciences, Beijing, 100190, China. and
University of Chinese Academy of Sciences, Beijing 100049, China.

A. Hoffmann

Material Science Division, Argonne National Laboratory, 9700 S. Cass Avenue, Lemont, IL 60439.

X. M. Liu and Z. M. Jin

Department of Physics, Shanghai University, Shanghai 200444, China.

Abstract: In tunnel junctions between ferromagnets and heavy elements with strong spin orbit coupling the magnetoresistance is usually dominated by tunneling anisotropic magnetoresistance (TAMR). This makes conventional DC spin injection techniques impractical for determining the spin relaxation time (τ_s). Here, we show that this obstacle for measurements of τ_s can be overcome by 2nd harmonic spin-injection-magnetoresistance (SIMR). In the 2nd harmonic signal the SIMR is comparable in magnitude to TAMR, thus enabling Hanle-induced SIMR as a powerful tool to directly determine τ_s. Using this approach we determined the spin relaxation time of Pt and Ta and their temperature dependences. The spin relaxation in Pt seems to be governed by Elliott-Yafet mechanism due to a constant resistivity×spin relaxation time product over a wide temperature range.

The remarkable applied potential of spin-orbit-torques for magnetic random access memory has stimulated intensive interest in investigating spin orbit coupling (SOC) in heavy metals such as Pt and Ta[1–11]. Their spin Hall angle (θ_SH), spin diffusion length (l_s) and spin relaxation time (τ_s), which influence switching efficiency are important parameters for determining their effectiveness, but especially the latter two are experimentally hard to assess. Accurate determination of τ_s could also help to identify the spin relaxation mechanisms[12]. Though θ_SH and l_s have been measured by spin pumping[13–17] and 2nd harmonic Hall measurement[18–20], τ_s of Pt and Ta is rarely reported. In principle, $\tau_\mathrm{s} = l_\mathrm{s}^2/D$, with D being the diffusion constant which is also difficult to determine independently.

Electron spin resonance (ESR) has been a standard technique to measure the spin relaxation time of bulk light metals[21]. However, it is not suitable for ultrathin films[22,23]. In addition, Elezzabi *et al.*[24] developed a time-resolved optical technique to directly measure the spin relaxation process in Au to be $\tau_\mathrm{s,Au} = (45 \pm 5)$ ps. However, this method is not suitable for heavy metals such as Pt, Ta and W with short τ_s[25]. Recently, Dyakonov[26] theoretically, then Vélez *et al.*[27] and Wu *et al.*[28] experimentally demonstrated a so-called Hanle magnetoresistance (MR) effect in Pt and Ta: a spin accumulation at the sample boundaries caused by the spin Hall effect is dephased by a magnetic field via the Hanle effect, which results in an additional positive MR. This electrical method can be applied to estimate τ_s from the magnetic field dependence[27,28]. Using this approach $\tau_\mathrm{s,Pt} =1.9$ ps was determined for Pt/SiO$_2$ and 0.61 ps

for Pt/YIG[28]. In fact, spin injection experiments in non-local spin valves[29–35] and 3-terminal geometries[36–40] are both powerful tools in measuring τ_s in metals and semiconductors. In these experiments, ferromagnetic layer (FM)/tunnel barrier/nonmagnetic layer (NM) junctions are adopted to both inject a non-equilibrium spin accumulation and simultaneously determine their magnitude. These measurement were used to determine spin relaxation times in a wide variety of materials, e.g., $\tau_{s,Si}$=55 - 285 ps for heavily doped silicon[40]; $\tau_{s,Graphene} > 1$ ns for graphene/BN[41]; $\tau_{s,Al}$=110 ps for aluminum[29], $\tau_{s,Cu}$=22 ps for copper[42] and $\tau_{s,Au}$=45 ps for gold[32].

However, it is impractical to apply these spin injection experiments to measure τ_s in heavy metals with strong SOC for at least two reasons. First, l_s in this case is so short (about several nanometers) that the preparation of nonlocal spin valves with comparable dimensions is beyond current lithography capabilities. Second, the real contact resistance is $r = r_C + r_{SI}$, where r_{SI} and r_C are the contact resistance induced by spin injection (SI) and the original contact resistance without r_{SI}, respectively. Here r_{SI} equals to $[r_N(p_C^2 r_C + p_F^2 r_F) + r_F r_C (p_F - p_C)^2]/r_{FN}$[12,43], in which $r_{FN} = r_F + r_N + r_C$, p_F is the spin polarization of FM and p_C is the spin polarization of the interfacial conductivity. The spin resistance in the NM(FM) layer $r_{N(F)}$ is defined as $\rho_{N(F)} l_{sN(F)}$. $\rho_{N(F)}$ and $l_{sN(F)}$ are the resistivity and spin diffusion length of NM(FM), respectively. Because $r_N, r_F \ll r_C$ for metals, $r \approx r_C + r_N p_C^2 + r_F (p_F - p_C)^2$. As one increases a field perpendicular to the spin polarization in the NM, the spin accumulation dephases. The dephasing process in NM and FM layer could be simulated by LLB equation whose results indicate that r_N vanishes due to the Hanle effect while the r_F is preserved by the effective field of about 10^7 Oe due to Heisenberg exchange coupling[44,45] and will not contribute to the field dependence of real contact resistance. This gives rise to a $MR \equiv [r(High\ field) - r(0)]/r(0) \approx -r_N p_C^2/r_C < 0$. This negative spin-injection-induced MR (SIMR) has

been utilized in 3-terminal geometries to measure τ_s in semiconductors[36–39] but is negligible in metallic systems, since $r_N \ll r_C$ by several orders of magnitude. Besides, r_C can also exhibit a field dependence due to SOC in FM/Barrier/NM junctions[46,47]. This so-called tunneling anisotropy MR (TAMR)[48] further complicates the analysis.

Here, we will show that even with a 3-terminal geometry, SIMR can be clearly observed by 2nd harmonic voltage measurements, since TAMR only dominates the 1st harmonic voltages. We adopted this method to determine τ_s in Pt and Ta and also their corresponding temperature dependences.

First we discuss the basic concept of these measurements. The tunneling conductance $g_C = 1/r_C$ is composed by counterparts for opposite spin channels, $g_C = g_{C\uparrow} + g_{C\downarrow}$. Here we have already neglected r_N and r_F in the contact resistance due to the fact that r_N, $r_F \ll r_C$. Spin injection into the NM or spin extraction from NM induces a non-equilibrium spin accumulation μ_N in NM, which increases or decreases Fermi levels of opposite spin channels. This can further lead to a change of g_C by $\triangle g_C = \frac{dg_{C\uparrow}}{dE}\mu_N - \frac{dg_{C\downarrow}}{dE}\mu_N = \frac{d(g_{C\uparrow} - g_{C\downarrow})}{dE}\mu_N$. The spin accumulation is given by $\mu_N = pr_N j$, where p and j are the tunneling spin polarization and current density across the junction[43]. Thus $\triangle g_C = \alpha pr_N j$ with $\alpha \equiv \frac{d(g_{C\uparrow} - g_{C\downarrow})}{dE}$. The voltage across the junction $v = r_C j$ is then

$$v = \frac{1}{(g_{C,0} + \triangle g_C)}j \approx (\frac{1}{g_{C,0}} - \frac{\triangle g_C}{g_{C,0}^2})j = \frac{1}{g_{C,0}}j - \frac{\alpha pr_N}{g_{C,0}^2}j^2$$
(1)

Here $g_{C,0}$ is the contact conductance at zero current, or $v = r_{C,0}j - \alpha pr_N r_{C,0}^2 j^2$ with $r_{C,0}$ being the contact resistance at zero current. $r_{C,0}$ does not contain SIMR. Assuming that $r_{C,0} = r_{C,00}(1 + TAMR)$ and $r_N = r_{N,0}(1 + SIMR)$, results in $v = r_{C,00}(1 + TAMR)j - \alpha pr_{N,0}r_{C,00}^2(1 + SIMR)(1 + TAMR)^2 j^2$, where $r_{C,00}$ and $r_{N,0}$ are the contact resistance and spin resistance at $H = 0$ and $j = 0$, respectively. This equation can be further reduced considering TAMR≪1 and SIMR≪1:

$$v \approx r_{C,00}(1 + \text{TAMR})j - \alpha p r_{N,0} r_{C,00}^2 (1 + \text{SIMR} + 2\text{TAMR})j^2 \qquad (2)$$

In practice, an AC current $j = j_0 \sin(\omega t)$ satisfying $\triangle g_C < g_{C,0}/10$ was selected to make the above Taylor expansion reasonable. Thus $v_{1\omega} = r_{C,00}(1 + \text{TAMR})j_0$ has no explicit dependence on SIMR while $v_{2\omega} = \frac{1}{2}\alpha p r_{N,0} r_{C,00}^2 (1 + \text{SIMR} + 2\text{TAMR})j_0^2$ has a dependence on both SIMR and 2TAMR. They also differ in phase by 90°. We would expect that TAMR dominates in $v_{1\omega}$ while SIMR becomes comparable to the TAMR and thus observable in $v_{2\omega}$ as shown in the following experiments.

Stacks of SiO_2// Ta(10) or Pt(10)/ MgO(2)/ $Co_{40}Fe_{40}B_{20}$(4)/ Ta(5)/ Ru(7) (thickness in nm) provided by Singulus Technologies AG were deposited via magnetron-sputtering and then post-annealed with a magnetic field of 1 T along the x-axis at 300 °C for 1 hour to induce an easy axis along the x-axis. M-H curves acquired by vibrating sample magnetometer (Microsense) showed in-plane magnetic anisotropy for both Ta/MgO/CoFeB and Pt/MgO/CoFeB stacks [Fig. 1(a) and (b)]. The anisotropy field of each sample is about 15 kOe along the z-axis, while the easy axis is along the x-axis. H_x smaller than 1 kOe is sufficient to align the magnetization along the easy axis.

The extended films were then processed into magnetic tunneling junctions by ultraviolet lithography and argon ion etching. The junctions had one top electrode (E1) and three bottom ones (E2, E3 and E4) [Fig. 1(c) and (d)]. The size of the junctions was 6 μm×6 μm. Ta/MgO/CoFeB or Pt/MgO/CoFeB junctions were surrounded by $MgAlO_x$ for protection and also for isolating E1 from the remaining electrodes. Magnetotransport properties were measured in a physical property measurement system (Quantum Design-9T). To measure the inverse spin Hall effect (ISHE) of the bottom electrodes, an AC current with sine wave and $f = \omega/2\pi = 8.7$ Hz was applied between E1 and E3 using a Keithley 6221

and the 1st harmonic voltage $V_{1\omega}$ between E2 and E4 was firstly pre-amplified (Stanford Research, SR560) and then picked up by a lock-in amplifier (SR830) [Fig. 1(d)].

In this setup, spin-polarized current was perpendicularly injected from the FM to the NM layer. Their spin orientation was along the x-axis at $|H_x| >$500 Oe. Then a voltage in the open circuit can be detected along the y-axis due to the ISHE. The field dependences of the 1st harmonic voltage $V_{1\omega}^{\text{ISHE}}$ between E2 and E4 in Ta and Pt junctions are illustrated in Fig. 1(e) and (f). The sign of $V_{1\omega}^{\text{ISHE}}$ reverses as expected with reversed sign of H_x. $V_{1\omega}^{\text{ISHE}}$ has opposite signs in the Ta and Pt due to their opposite θ_{SH}[49,50], which indicates successful spin injection into the bottom heavy metal layer. Similar ISHE behaviors in both junctions have also been observed near room temperature. The maximum $V_{1\omega}^{\text{ISHE}}/j_0$ of Ta and Pt junctions is about 1 mΩ and 0.1 mΩ at 300 K, which is in the same order of magnitude as in Ref. [51].

3-terminal MR measurements are further performed on both Ta and Pt junctions. We have first detected the 1st harmonic voltage $V_{1\omega}^{3T}$ between E1 and E4 with an AC current applied between E1 and E3 [inset of Fig. 2(a)]. $\text{TMR}_{1\omega}$ is defined as $[V_{1\omega}^{3T}(H)\text{-}V_{1\omega}^{3T}(0)]/V_{1\omega}^{3T}(0)$ and its field dependences is shown in Fig. 2(a)-(d). The MR originates from the tunneling junction instead of the anisotropy magnetoresistance (AMR) of the CoFeB layer. Direct measurements of AMR of the Ta/MgO/CoFeB and Pt/MgO/CoFeB stacks showed negligible field dependence in the 1st and 2nd harmonic measurements. AMR only appears in the DC measurement, whose value is only about 0.05% at room temperature. Bear in mind that the resistance of the tunnel junction is much higher than the resistance of the CoFeB thin film. Thus the voltage variation caused by the AMR of the CoFeB film only is too tiny to explain the field-dependence of $V_{1\omega}^{3T}$. Here the TMR is mainly attributed to anisotropic tunneling
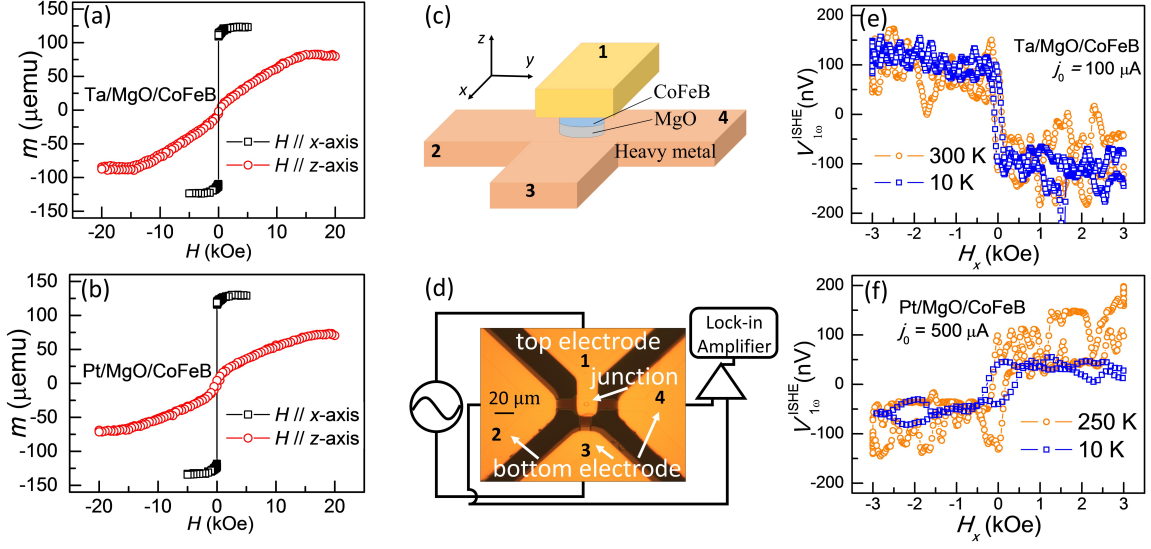
FIG. 1: (Color online) (a) and (b) Magnetic moment m vs H curve of Ta/ MgO/CoFeB and Pt/ MgO/CoFeB film. (c) Schematic of heavy metal/ MgO/$Co_{40}Fe_{40}B_{20}$ junctions. Top electrode 1 (E1) and bottom electrodes 2, 3 and 4 (E2, E3 and E4) are on opposite sides of 40-nm $MgAlO_x$ around the tunnel junction area. (d) The ISHE measurement setup applying an AC current between E1 and E3 and detecting the voltage between E2 and E4 with preamplifier and lock-in amplifier. (e) and (f) 1st harmonic ISHE voltage of Ta/ MgO/CoFeB and Pt/ MgO/CoFeB. High temperature (orange circle) or low temperature (blue) data are shown together for the Ta and Pt stacks, respectively. The current amplitude is 100 μA for Ta and 500 μA for Pt. Opposite field dependencies (e) and (f) indicate different signs of θ_{SH} of Ta and Pt.

magnetoresistance (TAMR) of the CoFeB/MgO/heavy metal junctions, and we use TAMR instead of TMR in the following analysis.

At high temperature, $TAMR_{1\omega}^z$ first quadratically increases as H_z increases from zero in both Ta and Pt junctions [Fig. 2(a) and (b)] and later gradually saturates at 0.20% for Ta and 0.14% for Pt junction as H_z approaches 15 kOe which is also the anisotropy field of the CoFeB layer. Further increasing H_z leads to a MR reduction for both junctions. When H_x is applied, $TAMR_{1\omega}^x$ increases only by about 0.01% and then decreases gradually toward the negative MR. Note that $TAMR_{1\omega}^z$ is much larger than $TAMR_{1\omega}^x$. H_z aligns the magnetization from in-plane to out-of-plane, which subsequently changes the density of state of the interfacial FM layer via SOC and results in TAMR as predicted theoretically[48,52]. The phenomenon

$TAMR_{1\omega}^z > TAMR_{1\omega}^x$ is consistent with Ref.[53], since H_x keeps the magnetization along the easy axis, and consequently $TAMR_{1\omega}^x$ varies little.

Similar behaviors are also observed at 10 K, except for larger saturation fields and slightly larger $TAMR_{1\omega}^z$ values [Fig. 2(c) and (d)]. The negative MR ,which depends on applied field instead of magnetization, is also observed at 10 K. For explicit discussion, the $v_{1\omega}$ vs H_z curve in Fig. 2(c) can be fitted with the three contributions as plotted in Fig. 3 as curve α, β and γ. The curve γ is the contribution of the mentioned negtive MR at large field. This MR might originate from suppression of electron-magnon scattering[54,55] or weak localization[56,57] of electrodes. Though detailed mechanism is still unclear, the negative MR is not rarely observed in this kind of HM/MgO/CoFeB structures. TAMR in the
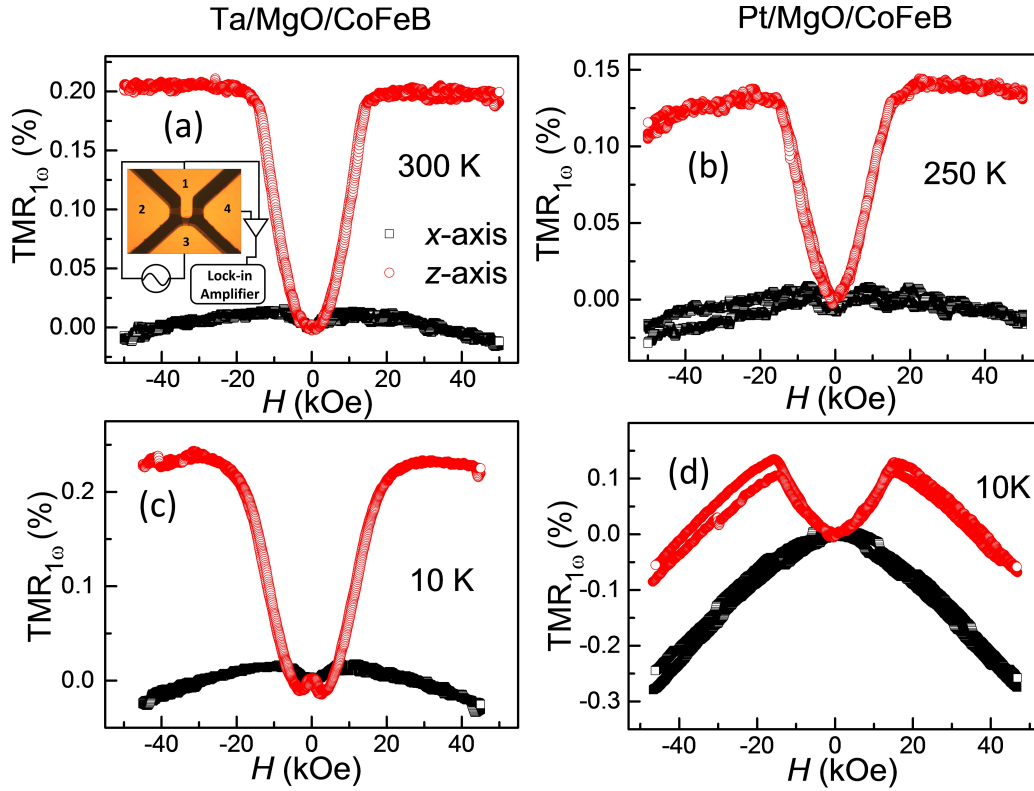
FIG. 2: (Color online) TMR obtained from 1st harmonic voltage with the 3-terminal (3T) measurement setup applying AC currents between E1 and E3 and detecting the voltages between E1 and E4 in the inset at high temperature (a) 300 K for Ta/MgO/CoFeB, (b) 250 K for Pt/MgO/CoFeB or low temperature 10 K for (c) Ta/MgO/CoFeB or (d) Pt/MgO/CoFeB. The external field is either in plane along x-axis (black square) or out of plane along z-axis (red circle). The currents are identical as in Fig. 1. (e) and (f), 100 μA for Ta/MgO/CoFeB [(a) or (c)] and 500 μA for Pt/MgO/CoFeB [(b) or (d)].
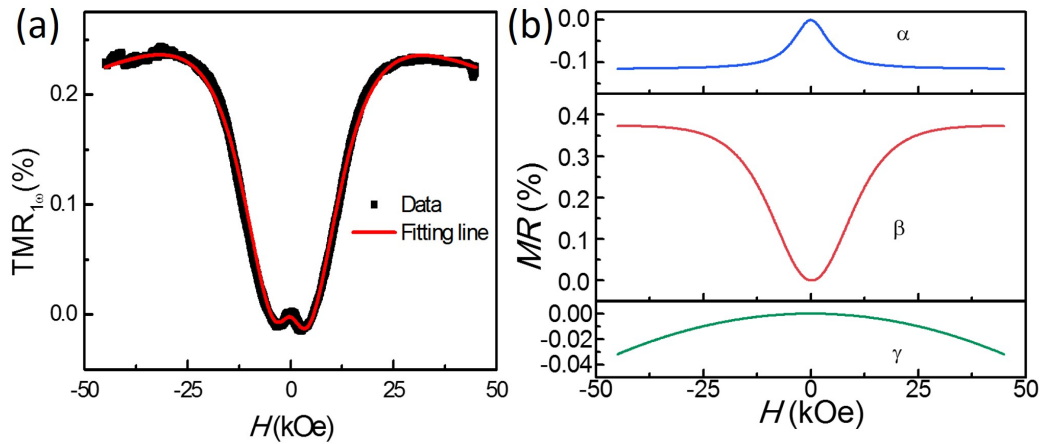

FIG. 3: (Color online) (a) The fitting of the $v_{1\omega}$ vs H_z curve. (b) Three contributions, Hanle effect (curve α), TAMR (curve β) and a negative MR (curve γ), are taken into account.

work of Park et $al.$[58] also declines after reaching a max-   imum at saturation field.The curve β, due to TAMR, is

highly relevant to magnetization and can be reproduced by $aR_{xy}^2(H)$ with a being the proportional coefficient. The curve α shows a small negative MR (about -0.014 %) appears at low H_z in the Ta junction, which is the only remarkable difference between the results of 10 K and high temperature. This negative MR exhibits a similar field dependence as the Hanle-effect-induced SIMR which would exhibit a Lorentzian-shape dependence as discussed next. Thus we attribute it to spin injection into Ta. This $SIMR_{1\omega}$ should have been negligibly small due to the fact $r_N \ll r_C$. In fact, it turns out to be unobservable in the Pt junction or at high temperatures. It might be possible that inhomogeneities of the MgO layer which is shown in Appendix A result in a significant reduction of the effective tunneling area and smaller r_C in the Ta junction. This may lead to a reemerging of $SIMR_{1\omega}$ although $SIMR_{1\omega}$ is still one order smaller than $TAMR_{1\omega}^z$. Inhomogeneous current distribution due to the resistance of the nonmagnetic layer within the junction area could reduce the measured tunneling resistance below the real tunneling resistance by about 10.8% and 4.5% for Ta and Pt junctions respectively due to device geometry as well as inhomogeneous current distribution within the junction[59,60]. However, this would not affect the injected spins and their dephasing process in the heavy metal layers. Therefore, this resistance adjustment would not physically influence the field dependence of the TAMR and the SIMR effects which is the basis of estimating the spin relaxation times.

$V_{2\omega}^{3T}$ was detected in the same setup as shown in the inset of Fig. 2(a). The only difference is that the 2nd harmonic voltage with 90° phase shift was measured with the lock-in amplifier. As shown in Eq. (2), SIMR should be comparable to TAMR within a factor of 2 for the 2nd harmonic signal. Thus this method renders Hanle and inverted Hanle effect signals induced by SIMR detectable even in the presence of a TAMR background (Fig. 4).

The field dependence of $V_{2\omega}^{3T}$ at 300 K or 250 K for Ta and Pt junction is shown in Fig. 3(a) and (b). For small H_z, the magnetization is still aligned along the easy axis. An AC current injects (extracts) spins into (from) NM and leads to a non-equilibrium spin accumulation, which conversely influences tunneling resistance and contributes an additional $V_{2\omega}$. A vertical H_z can dephase the spin accumulation via the Hanle effect and therefore diminish the additional $V_{2\omega}$, leading to a negative MR with a Lorentzian shape in the 2nd harmonic signal. This Hanle dephasing is the same as established by Silsbee[61] for DC measurement. It is worth noting that $TAMR_{2\omega}$ and $SIMR_{2\omega}$ contribute to a positive and negative MR, respectively. In addition, $TAMR_{2\omega}$ as well as curve γ has a H_z^2 dependence at low field. Thus by fitting $V_{2\omega}$ vs. H_z curves with a Lorentzian function plus a H_z^2 function, we can obtain a spin relaxation time $\tau_s = e/(mB_0)$ with the electron charge e, electron mass m and B_0 being the half width at half maximum of the Lorentzian fitting. τ_s is (7.8±1.6) ps at 300 K and (13.1±0.6) ps at 10 K for Ta [Fig. 4(a) and (b)]. By further increasing H_z beyond 10 kOe, $V_{2\omega}^{3T}$ increases due to both tilting of magnetization and the concomitant TAMR contribution.

In contrast, H_x avoids dephasing of the spin polarization along x, and therefore extends spin relaxation process and finally causes a positive MR in small field. This picture accounts for the inverted Hanle effect[40]. A similar positive SIMR also occurs as applying H_x for the 2nd harmonic signal (Fig. 4). Besides, $V_{2\omega}$ exhibits a $H_{z/x}$ dependence at high fields, especially at 10 K, but the origin of this field dependence is unclear at this point. The Hanle signal in Fig. 4 (c) and (d) results in τ_s (5.0±1.5) ps at 250 K and (7.3±0.6) ps at 10 K for Pt. The inverted Hanle SIMR shows similar behavior for Ta. More than 4 devices are measured to estimate the τ_s for each type of stacks.

In order to investigate the temperature (T) dependence of τ_s, we have conducted the 2nd harmonic SIMR measurement in a Hanle geometry at different temperatures [Fig. 5(a) and (b)]. As T decreases from 300 K to 10 K, the Hanle-effect-induced $\triangle V_{2\omega}$ grows significantly
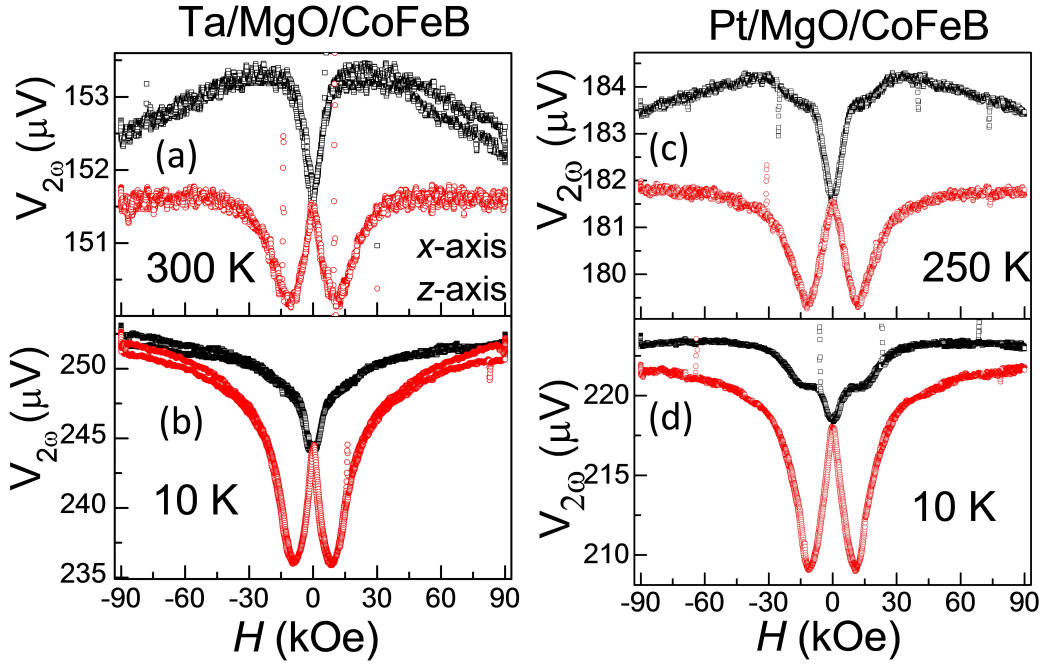
FIG. 4: (Color online) 2nd harmonic voltage with the 3-terminal (3T) measurement setup for Ta/MgO/CoFeB at (a) 300 K or (b) 10 K, and for Pt/MgO/CoFeB at (c) 250 K or (d) 10 K. The magnetic field was applied along the x-axis (black square) for inverted Hanle measurement or the z-axis (red circle) for Hanle measurement.

by nearly one order of magnitude. In order to examine whether the field range for selecting the data affects B_0, we have tried different ranges (±13 kOe, ±14 kOe and ±15 kOe) for the fitting. The T dependence is basically the same for different fitting ranges. Their variance is less than 2 ps for both materials. Taking the ±14 kOe fitting range, τ_s in Ta gradually decays from (13.1 ± 0.6) ps at 10 K to (7.8 ± 1.6) ps at 300 K. In contrast, if the H^2 correction is ignored in the fitting τ_s stays at 20 ps below 150 K and then decays to 14 ps at 300 K. These values are not only 50% higher than those with H^2 correction but also exhibits an unreasonable T dependence. Thus the H^2 correction is indispensable. τ_s of Pt and Ta is about 10 ps or below. These values are 1-3 orders smaller than τ_s in light metals or semiconductors, consistent with the trend that elements with larger atomic number have stronger SOC. $\tau_{s,Pt}$ is about half of $\tau_{s,Ta}$ at all temperatures in our experiment and much smaller than $\tau_{s,Au}$ of 45 ps. Here $\tau_{s,Pt}=(5.0\pm1.5)$ ps at 250 K is about twice of 1.9 ps

measured by Hanle MR, which might be caused by lower resistivity in the former Pt and different film thickness in the two experiments. In our experiment, $\rho_{Pt}=24.4$ $\mu\Omega$cm at 300 K, while it is 58 $\mu\Omega$cm in Ref.[28]. $\tau_s\rho$ appears to be a constant for these two samples. The T dependence of ρ_{Pt} and ρ_{Ta} is also measured. For resistivity measurement, the top structure MgO/CoFeB/capping layers in the Pt/MgO/CoFeB or Pt/MgO/CoFeB stacks are etched away. ρ_{Pt} decreases weakly with decreasing temperature and $\tau_s\rho$ in Pt is nearly a constant from 300 K to 10 K for all the fitting ranges [Fig. 5(f)]. The momentum relaxation time τ_p is inversely proportional to ρ. Thus τ_s/τ_p is also a constant, which indicates that the spin relaxation in Pt is governed by Elliott-Yafet mechanism [12]. We also applied a THz technique[62] to directly measure momentum relaxation time and resistivity of Pt with 30 nm thickness, which gives $\tau_p=(5\pm3)$ fs and $\rho_{Pt}=16$ $\mu\Omega$cm at 300 K. Assuming that τ_p is proportional to $1/\rho_{Pt}$, τ_p in our Pt/MgO/CoFeB stacks is thus around 2.7 fs. There-
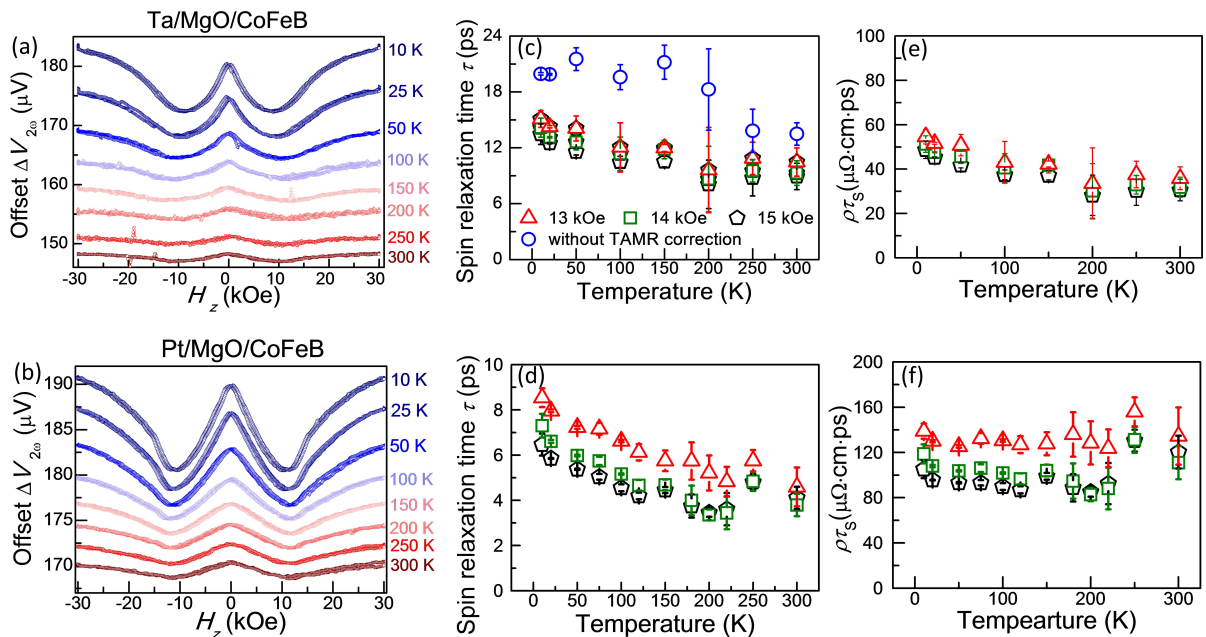
FIG. 5: (Color online) Temperature dependence of the 2nd harmonic voltage of Hanle measurements for (a) Ta/MgO/CoFeB and (b) Pt/MgO/CoFeB from 10 K to 300 K. And temperature dependence of spin relaxation time (c) for Ta/MgO/CoFeB and (d) for Pt/MgO/CoFeB acquired via fitting the data with a Lorentzian curve plus a parabolic function for the TAMR correction applied in different field ranges ±13 Oe (red triangle), ±14 Oe (olive square) and ±15 Oe (black pentagon) or without the parabolic function fitting (blue circle). (e) shows that $\tau_s\rho$ of Pt remains nearly constant from 300 K to 10 K for all fitting ranges.(f)Temperature dependence of $\tau_s\rho$ of Ta.

fore the spin flip probability of each scattering τ_p/τ_s is around 7×10^{-4} for Pt at 300 K.

Our ρ_{Ta} is about 342 $\mu\Omega$cm at 300 K, much larger than those reported for the resistivity of α-phase and even β-phase Ta or amorphous Ta[63–68], which might be due to oxidation of Ta after the top structure is etched. Schwartz et al.[66] reported the a resistivity at room temperature of 200±20 $\mu\Omega$cm and a temperature coefficient of resistance (TCR) from 200 K to 300 K of -175 to -178 p.p.m. / K for beta Ta. Before his work, Schauer et al.[65] also reported a TCR of about-100 p.p.m./K for beta Ta. In 2006, Narayan et al.[67]reported a room-temperature resistivity of 275 $\mu\Omega$cm for amorphous Ta and the negative TCR of about -205 p.p.m./K. According to Naranyan et al.[67] and Stella et al.[68], the amorphous Ta has higher resistivity (above 200 $\mu\Omega$cm) and negative TCR. In our films, the TCR is -198 p.p.m. / K for Ta film. Although

the TCR of our sample is in the same level of the reported ones, the resistivity is too high to eliminate the posibility of oxidation. The interface oxidation layer would make the effective cross-section area less than the nominal one which is used to calculate the resistivity, which would enlarge the resistivity but not TCR of the films because the oxide Tantalum nearly do not participate in the electrical transport. Therefore $\rho_{Ta}\tau_{s,Ta}$ vs. T shown in Fig. 5(e) is not used here for examining the spin relaxation mechanism.

In conclusion, TAMR$_{1\omega}$ dominates the 1st harmonic 3-terminal MR measurement while SIMR$_{2\omega}$ becomes significant compared to the TAMR$_{2\omega}$ background and turns out to be much easier measured in the 2nd than in the 1st harmonic signal. This renders conventional 3-terminal FM/barrier/NM devices suitable for directly measuring the spin relaxation time τ_s of heavy metals without com-

plications from proximity effects[69–72] that occur, when the heavy metal is in direct contact with a ferromagnet. ISHE is also observed, which proves successful spin injection into Ta and Pt. By fitting Hanle curves with a Lorentzian function plus a parabolic TAMR background, we have obtained τ_s of Ta and Pt. The τ_s for both materials exhibits a small increase from 300 K to 10 K, such that τ_s is about (7.8±1.6) ps and (5.0±1.5) ps for Ta and Pt at high temperature while it is about (13.1±0.6) ps and (7.3±0.6) ps at 10 K, respectively. Since $\tau_s\rho$ stays constant at all temperatures, the spin relaxation in Pt seems to be dominated by the Elliott-Yafet mechanism. This experimental approach provides an electrical manner to directly quantify spin relaxation time of heavy metals, which have been elusive from conventional SIMR or optical measurements. Furthermore, there is no physical limitation for this method to be generalized to other light metals and semiconductors.

I. ACKNOWLEDGMENTS

II. APPENDIX

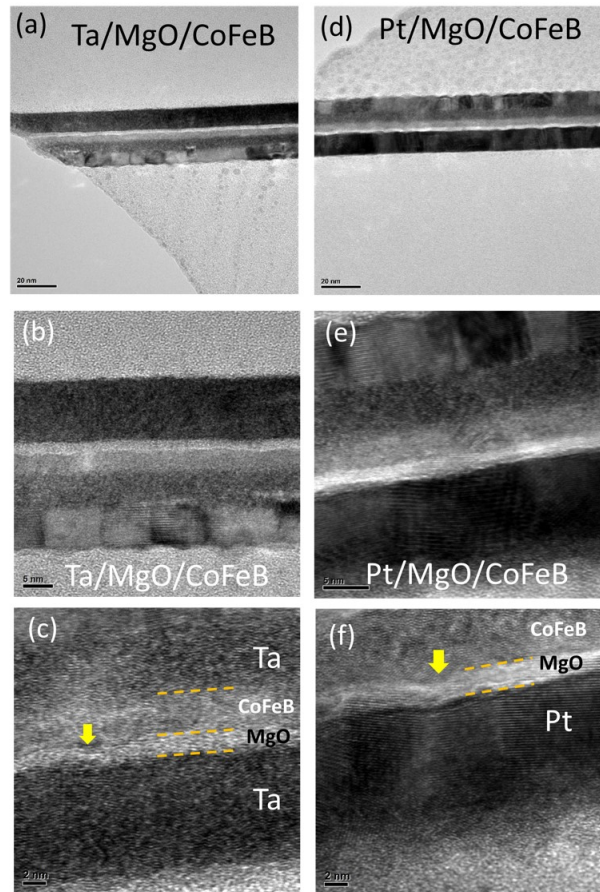## Appendix A: A. TEM characterization of cross section of junctions

Fig. A1(Color online) (a),(b)and(c) TEM pattern of the cross section of Ta/MgO/CoFeB stacks in different scale. (d),(e)and(f) TEM pattern of the cross section of Pt/MgO/CoFeB stacks in different scale. Yellow arrows in the patterns point to the inhomogeneous area of the MgO barrier.

TEM pictures (Fig. A1) show good quality of the MgO layer with clear and flat interfaces in a large scale (Fig. A1 (a),(b) for Ta/MgO/CoFeB stacks and (d),(e) for Pt/MgO/CoFeB stacks), demonstrating that a portion of samples, at least in probability, are good enough for direct tunneling to dominate the field dependence of the junction resistance in the harmonic measurement. This

means multi-measurement in different samples would be helpful to obtain more reliable τ values.

Nevertheless, Fig. A1(c)and(f) also shows that the MgO thickness in some region is not very uniform. The yellow arrows point out the area where the thickness is less than surrounding area and could probably act as the inhomogeneous area which leads to a larger tunneling rate and may account for a reduction of the effective tunneling area.

Appendix B: B. $I - V$ characteristics

This section shows the $I - V$ characteristics of Ta/MgO/CoFeB and Pt/MgO/CoFeB junctions at room temperature (Fig. A2(a) and (b)).
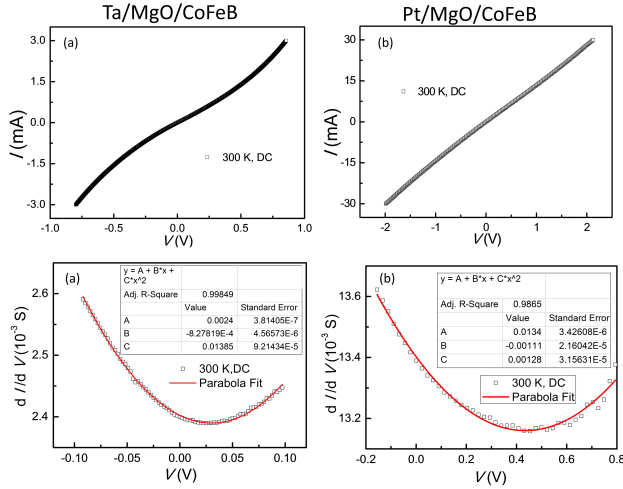

Fig. A2(Color online) $I - V$ curve of (a) Ta/MgO/CoFeB and (b) Pt/MgO/CoFeB junctions at room temperature Voltage dependence of conductance of (a) Ta/MgO/CoFeB and (b) Pt/MgO/CoFeB junctions at room temperature at low voltage. The red line is parabolic fitting whose parameter is shown in the table in the figures.

Brinkman et al. (BDR fit)[73] gave the equation for the conductivity of the metal-insulator-metal junctions as $(G(V))/(G(0)) = 1 - AV + BV^2$ at low voltages, in which

A and B are material related parameters. The equation indicates that the plot of conductivity versus voltage will be a parabolic function. We adopt the Parabolic fitting to our $dI/dV - V$ data as shown in Fig. A2 (c)and(d). The data show good fitting outcome, indicating tunneling mechanism dominates transport properties of the junctions.

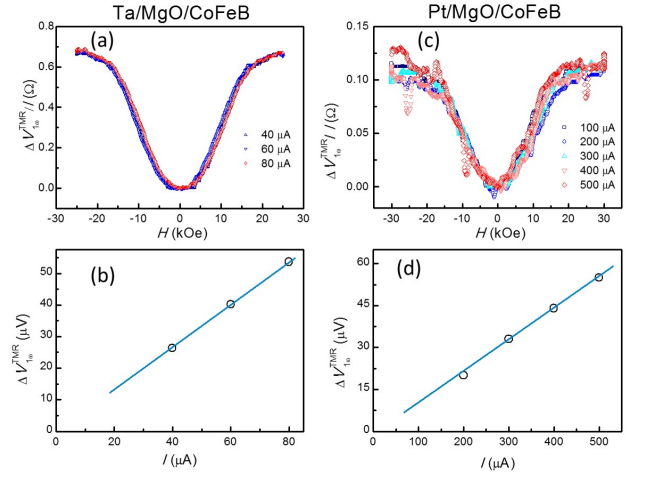## Appendix C: C. The current dependence of first and second harmonic voltage

Fig. A3(Color online) (a, c) The field dependence of $\Delta V_{1\omega}^{\mathrm{TMR}}/I$ under different applied current, (b, d) The dependence of $\Delta V_{1\omega}^{\mathrm{TMR}}$ on the applied current for Ta/MgO/CoFeB samples(a, b) and Pt/MgO/CoFeB samples(c, d).

We measured the current dependence of first and second harmonic voltage shown in Fig. A3 and Fig. A4 to demonstrate that the first and second harmonic voltage variation are proportional to j and j^2 respectively. The obtained τ_s stays almost the same in the current ranges we used for both Ta and Pt samples. Due to much lower signal-to-noise ratio at small measurement current, τ_s shows some abnormality in this region, which we think is not physical.
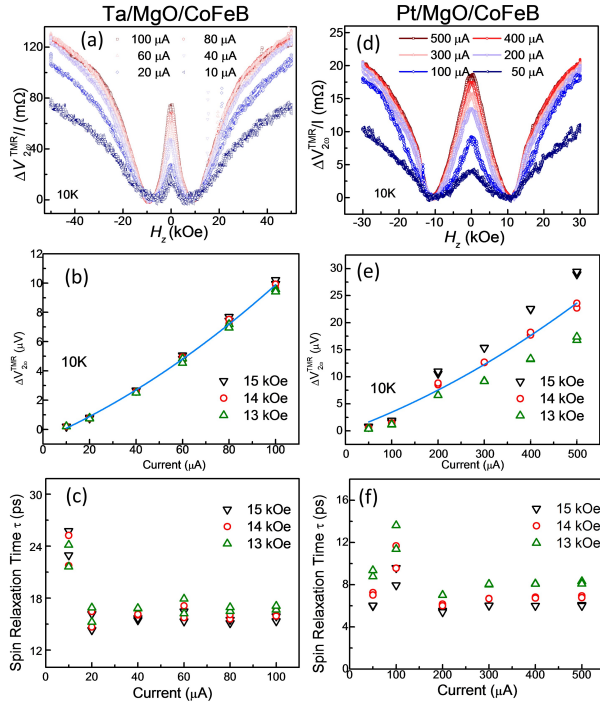
Fig. A4(Color online) (a, c) The field dependence of $\Delta V_{2\omega}^{\mathrm{TMR}}/I$ under different applied current, (b, e) The current dependence of $\Delta V_{2\omega}^{\mathrm{TMR}}$ and (c, f) the τ measured at different currents for Ta/MgO/CoFeB samples(a, b, c) and Pt/MgO/CoFeB samples(d, e, f).

* wancaihua@iphy.ac.cn

† xfhan@iphy.ac.cn

[1] C. O. Avci, K. Garello, I. M. Miron, G. Gaudin, S. Auffret, O. Boulle, and P. Gambardella, Appl. Phys. Lett. **100**, 212404 (2012).

[2] G. Finocchio, M. Carpentieri, E. Martinez, and B. Azzerboni, Appl. Phys. Lett. **102**, 212410 (2013).

[3] E. Martinez, S. Emori, and G. S. D. Beach, Appl. Phys. Lett. **103**, 072406 (2013).

[4] C. H. Sim, J. C. Huang, M. Tran, and K. Eason, Appl. Phys. Lett. **104**, 012408 (2014).

[5] P. V. Ong, N. Kioussis, P. K. Amiri, K. L. Wang, and G. P. Carman, J. Appl. Phys. **117**, 17B518 (2015).

[6] P. M. Haney, H. W. Lee, K. J. Lee, A. Manchon, and M. D. Stiles, Phys. Rev. B **88**, 214417 (2013).

[7] K. K. Meng, J. Miao, X. G. Xu, J. X. Xiao, J. H. Zhao, and Y. Jiang, Phys. Rev. B **93**, 060406 (2016).

[8] S. Y. Huang, X. Fan, D. Qu, Y. P. Chen, W. G. Wang, J. Wu, T. Y. Chen, J. Q. Xiao, and C. L. Chien, Phys. Rev. Lett. **109**, 107204 (2012).

[9] A. Hoffmann and S. D. Bader, Phys. Rev. Appl. **4**, 047001 (2015).

[10] W. J. Kong, Y. R. Ji, X. Zhang, H. Wu, Q. T. Zhang, Z. H. Yuan, C. H. Wan, X. F. Han, T. Yu, K. Fukuda, H. Naganuma, and M. J. Tung, Appl. Phys. Lett. **109**, 132402 (2016).

[11] X. Zhang, C. H. Wan, Z. H. Yuan, Q. T. Zhang, H. Wu, L. Huang, W. J. Kong, C. Fang, U. Khan, and X. F. Han, Phys. Rev. B **94**, 174434 (2016).

[12] I. Zutic, J. Fabian, and S. Das Sarma, Rev. Mod. Phys. **76**, 323 (2004).

[13] W. Zhang, V. Vlaminck, J. E. Pearson, R. Divan, S. D.

Bader, and A. Hoffmann, Appl. Phys. Lett. **103**, 242414 (2013).

[14] O. Mosendz, V. Vlaminck, J. E. Pearson, F. Y. Fradin, G. E. W. Bauer, S. D. Bader, and A. Hoffmann, Phys. Rev. B **82**, 214403 (2010).

[15] V. Vlaminck, J. E. Pearson, S. D. Bader, and A. Hoffmann, Phys. Rev. B **88**, 064414 (2013).

[16] O. Mosendz, J. E. Pearson, F. Y. Fradin, G. E. W. Bauer, S. D. Bader, and A. Hoffmann, Phys. Rev. Lett. **104**, 046601 (2010).

[17] J. C. Rojas-Sanchez, N. Reyren, P. Laczkowski, W. Savero, J. P. Attane, C. Deranlot, M. Jamet, J. M. George, L. Vila, and H. Jaffres, Phys. Rev. Lett. **112**, 106602 (2014).

[18] S. Woo, M. Mann, A. J. Tan, L. Caretta, and G. S. D. Beach, Appl. Phys. Lett. **105**, 212404 (2014).

[19] K. Garello, I. M. Miron, C. O. Avci, F. Freimuth, Y. Mokrousov, S. Blugel, S. Auffret, O. Boulle, G. Gaudin, and P. Gambardella, Nat. Nanotechnol. **8**, 587 (2013).

[20] H. Reichlova, D. Kriegner, V. Holy, K. Olejnik, V. Novak, M. Yamada, K. Miura, S. Ogawa, H. Takahashi, T. Jungwirth, and J. Wunderlich, Phys. Rev. B **92**, 165424 (2015).

[21] P. Monod and F. Beuneu, Phys. Rev. B **19**, 911 (1979).

[22] S. Schultz and C. Latham, Phys. Rev. Lett. **15**, 148 (1965).

[23] R. B. Lewis and T. R. Carver, Phys. Rev. **155**, 309 (1967).

[24] A. Y. Elezzabi, M. R. Freeman, and M. Johnson, Phys. Rev. Lett. **77**, 3220 (1996).

[25] P. Riego, S. Vlez, J. M. Gomez-Perez, J. A. Arregi, L. E. Hueso, F. Casanova, and A. Berger, Appl. Phys. Lett. **109**, 172402 (2016).

[26] M. I. Dyakonov, Phys. Rev. Lett. **99**, 126601 (2007).

[27] S. Vélez, V. N. Golovach, A. Bedoya-Pinto, M. Isasa, E. Sagasta, M. Abadia, C. Rogero, L. E. Hueso, F. S. Bergeret, and F. Casanova, Phys. Rev. Lett. **116**, 016603 (2016).

[28] H. Wu, X. Zhang, C. H. Wan, B. S. Tao, L. Huang, W. J. Kong, and X. F. Han, Phys. Rev. B **94**, 174407 (2016).

[29] M. Johnson and R. H. Silsbee, Phys. Rev. Lett. **55**, 1790 (1985).

[30] F. J. Jedema, A. T. Filip, and B. J. van Wees, Nature **410**, 345 (2001).

[31] F. J. Jedema, H. B. Heersche, A. T. Filip, J. J. A. Baselmans, and B. J. van Wees, Nature **416**, 713 (2002).

[32] J. H. Ku, J. Chang, H. Kim, and J. Eom, Appl. Phys.

Lett. **88**, 172510 (2006).

[33] O. M. J. van't Erve, A. T. Hanbicki, M. Holub, C. H. Li, C. Awo-Affouda, P. E. Thompson, and B. T. Jonker, Appl. Phys. Lett. **91**, 212109 (2007).

[34] Y. Ji, A. Hoffmann, J. S. Jiang, and S. D. Bader, Appl. Phys. Lett. **85**, 6218 (2004).

[35] Y. Ji, A. Hoffmann, J. E. Pearson, and S. D. Bader, Appl. Phys. Lett. **88**, 052509 (2006).

[36] S. P. Dash, S. Sharma, R. S. Patel, M. P. de Jong, and R. Jansen, Nature **462**, 491 (2009).

[37] K. R. Jeon, B. C. Min, I. J. Shin, C. Y. Park, H. S. Lee, Y. H. Jo, and S. C. Shin, Appl. Phys. Lett. **99**, 199902 (2011).

[38] X. Lou, C. Adelmann, M. Furis, S. A. Crooker, C. J. Palmstrom, and P. A. Crowell, Phys. Rev. Lett. **96**, 176603 (2006).

[39] T. Uemura, K. Kondo, J. Fujisawa, K. Matsuda, and M. Yamamoto, Appl. Phys. Lett. **101**, 132411 (2012).

[40] S. P. Dash, S. Sharma, J. C. Le Breton, J. Peiro, H. Jaffres, J. M. George, A. Lemaitre, and R. Jansen, Phys. Rev. B **84**, 054410 (2011).

[41] S. Singh, J. Katoch, J. S. Xu, C. Tan, T. C. Zhu, W. Amamou, J. Hone, and R. Kawakami, Appl. Phys. Lett. **109**, 122411 (2016).

[42] S. Garzon, I. Žutić, and R. A. Webb, Phys. Rev. Lett. **94**, 176601 (2005).

[43] A. Fert and H. Jaffrès, Phys. Rev. B **64**, 184420 (2001).

[44] B. D. Cullity and C. D. Graham, "Ferromagnetism," in *Introduction to Magnetic Materials* (John Wiley & Sons, Inc., 2008) pp. 115–149.

[45] I. M. Miron, K. Garello, G. Gaudin, P. J. Zermatten, M. V. Costache, S. Auffret, S. Bandiera, B. Rodmacq, A. Schuhl, and P. Gambardella, Nature **476**, 189 (2011).

[46] A. Matos-Abiague and J. Fabian, Phys. Rev. B **79**, 155303 (2009).

[47] O. Txoperena, M. Gobbi, A. Bedoya-Pinto, F. Golmar, X. N. Sun, L. E. Hueso, and F. Casanova, Appl. Phys. Lett. **102**, 192406 (2013).

[48] C. Gould, C. Ruster, T. Jungwirth, E. Girgis, G. M. Schott, R. Giraud, K. Brunner, G. Schmidt, and L. W. Molenkamp, Phys. Rev. Lett. **93**, 117203 (2004).

[49] C. Hahn, G. de Loubens, O. Klein, M. Viret, V. V. Naletov, and J. Ben Youssef, Phys. Rev. B **87**, 174417 (2013).

[50] A. Hoffmann, IEEE Trans. Magn. **49**, 5172 (2013).

[51] L. Liu, C.-T. Chen, and J. Z. Sun, Nat. Phys. **10**, 561 (2014).

[52] H. Saito, S. Yuasa, and K. Ando, Phys. Rev. Lett. **95**, 086604 (2005).

[53] S. Hatanaka, S. Miwa, K. Matsuda, K. Nawaoka, K. Tanaka, H. Morishita, M. Goto, N. Mizuochi, T. Shinjo, and Y. Suzuki, Appl. Phys. Lett. **107**, 082407 (2015).

[54] B. Raquet, M. Viret, E. Sondergard, O. Cespedes, and R. Mamy, Phys. Rev. B **66**, 024433 (2002).

[55] P. V. P. Madduri and S. N. Kaul, Phys. Rev. B **95**, 184402 (2017).

[56] G. Bergmann, Phys. Rep. **107**, 1 (1984).

[57] R. S. Markiewicz and C. J. Rollins, Phys. Rev. B **29**, 735 (1984).

[58] J.-Y. Park, S.-h. C. Baek, S.-Y. Park, Y. Jo, and B.-G. Park, Appl. Phys. Lett. **107**, 182407 (2015).

[59] R. J. Pedersen and F. L. Vernon, Appl. Phys. Lett. **10**, 29 (1967).

[60] J. S. Moodera, L. R. Kinder, J. Nowak, P. LeClair, and R. Meservey, Appl. Phys. Lett. **69**, 708 (1996).

[61] M. Johnson and R. H. Silsbee, Phys. Rev. B **37**, 5326 (1988).

[62] Z. M. Jin, A. Tkach, F. Casper, V. Spetter, H. Grimm, A. Thomas, T. Kampfrath, M. Bonn, M. Klaui, and D. Turchinovich, Nat. Phys. **11**, 761 (2015).

[63] M. H. Read and C. Altman, Appl. Phys. Lett. **7**, 51 (1965).

[64] L. A. Clevenger, A. Mutscheller, J. M. E. Harper, C. Cabral, and K. Barmak, J. Appl. Phys. **72**, 4918 (1992).

[65] A. Schauer, W. Peters, and W. Juergens, Thin Solid Films **8**, R9 (1971).

[66] N. Schwartz, W. A. Reed, P. Polash, and M. H. Read, Thin Solid Films **14**, 333 (1972).

[67] J. Narayan, V. Bhosle, A. Tiwari, A. Gupta, P. Kumar, and R. Wu, J. Vac. Sci. Technol. A **24**, 1948 (2006).

[68] K. Stella, D. Buerstel, S. Franzka, O. Posth, and D. Diesing, J. Phys. D: Appl. Phys. **42**, 135417 (2009).

[69] G. Y. Guo, Q. Niu, and N. Nagaosa, Phys. Rev. B **89**, 214406 (2014).

[70] J. Vogel, A. Fontaine, V. Cros, F. Petroff, J. P. Kappler, G. Krill, A. Rogalev, and J. Goulon, Phys. Rev. B **55**, 3663 (1997).

[71] F. Wilhelm, P. Poulopoulos, G. Ceballos, H. Wende, K. Baberschke, P. Srivastava, D. Benea, H. Ebert, M. Angelakeris, N. K. Flevaris, D. Niarchos, A. Rogalev, and N. B. Brookes, Phys. Rev. Lett. **85**, 413 (2000).

[72] W. Zhang, M. B. Jungfleisch, W. J. Jiang, Y. H. Liu, J. E. Pearson, S. G. E. te Velthuis, A. Hoffmann, F. Freimuth, and Y. Mokrousov, Phys. Rev. B **91**, 115316 (2015).

[73] W. F. Brinkman, R. C. Dynes, and J. M. Rowell, J. Appl. Phys. **41**, 1915 (1970).